Optics Communications 465 (2020) 125604

Contents lists available at ScienceDirect

Optics Communications

journal homepage: www.elsevier.com/locate/optcom

THz narrow band-pass filter based on stopband modulation in corrugated parallel plate waveguides

Kehui Jia [a,*], Lina Fan [b], Zhaoliang Cao [c]

[a] Solar Energy Research Center, School of Electronic Information Engineering, Suzhou Vocational University, Suzhou 215104, China
[b] School of Optics-Electrical and Computer Engineering, University of Shanghai for Science and Technology, Shanghai 200093, China
[c] State Key Laboratory of Applied Optics, Changchun Institute of Optics, Fine Mechanics and Physics, Chinese Academy of Sciences, Changchun 130033, China

ARTICLE INFO

Keywords:
Band-pass filters
Stopband
Terahertz wave
Spatial filters
Wave propagation

ABSTRACT

We demonstrate stopband modulation in a corrugated parallel plate waveguide (PPWG) in terahertz (THz) frequency. Different from the traditional approaches to achieve narrow band-pass filter, a method based on the junction of two stopbands is provided. Two stopbands can come closer through adjustment of plate distance and controlling the grooves depth, which generate a narrowband transmission region. It is found that plate distance can control the interval of two stopbands. On optimization of plate distance, the filter can achieve a range of zero-sideband, high transmissivity (T=99.8%), narrow linewidth (5.8 GHz), and high-quality factor (Q≈220). Furthermore, we also present the designs of tunable filter and modulate performance when liquid crystal (LC) is used as waveguide material. So, an excellent tunable filtering characteristic has been achieved. Finally, this work provides a new possibility for the designing of narrow band-pass filter devices.

1. Introduction

The parallel plate waveguide (PPWG) is an effective wavelength or frequency selection device which can improve the imaging quality of terahertz (THz) high-resolution imaging. Because the passive devices can easily couple free-space THz wave and exhibit low transmission loss [1–3]. The bandgap properties of PPWG can be easily understood. At certain frequency range, the stopband can hinder the electromagnetic energies or wave vectors to reach the end of the corrugated PPWG. PPWG has been used in novel optical and electronic devices, particularly in the field of waveguiding and filtering-based bandgap properties. Recently, most of the related research is focused on the band-stop filter which utilizes its structure configuration [4–6], with resonance dip in THz frequency. In contrast, PPWG geometry was seldom used to develop a band-pass filter device. Recently, several interesting studies were conducted; an experimental study on narrow band-pass high-contrast frequency filtering has been reported which incorporates two-dimensional cylinder structures into the metal PPWG [7]. Moreover, around 1 THz frequency narrow-band terahertz filter with 2 GHz passband linewidth was proposed, they also introduced point and line defects within periodic structure [8]. All of the reported work has its own advantage and based on this a similar PPWG structure has been investigated. However, we report a new method to achieve narrow band-pass filter, controlling the stopband of THz wave transmission in PPWG.

In a PPWG device, multiple transmission modes are possible. The PPWG can support two kinds of electromagnetic modes: coupled surface plasmon-polariton (SPP) modes [9,10] and conventional waveguide modes [11,12]. The plate distance and grooves depth of PPWG are important factors that are responsible for the complex mixed modes of PPWG [13,14]. In addition, strong hybridization and adjustability of SPP and waveguide mode along with the modifications of these two factors have been showed [15,16]. The interval of multiple transmission modes forms stopbands (bandgaps), which generally exhibit a sharp cutoff, a passband lies in the region between two stopbands. One promising method can perfect the passband, utilizing the modulation of two stopbands based on the metal PPWG structure. Moreover, this can be utilized for the construction of a filter with an exceptionally narrow transmission band. In this work, we investigate stopband characteristics and the design of a band-pass filter in a corrugated PPWG in THz frequency. The THz system requires dynamic control of the guided THz signal. We also discuss the tuning characteristic by controlling the refractive index of dielectrics inside a longitudinal metal PPWG.

2. Proposed model and characteristics of the conventional spectrum

Schematic diagram of the proposed model is given in Fig. 1. In this model, two thin metal plates with a thickness t are closely placed to each other which form one PPWG. Silver is used as plate material which

* Corresponding author.
E-mail address: jiakehui@jssvc.edu.cn (K. Jia).

https://doi.org/10.1016/j.optcom.2020.125604
Received 17 October 2019; Received in revised form 6 February 2020; Accepted 25 February 2020
Available online 26 February 2020

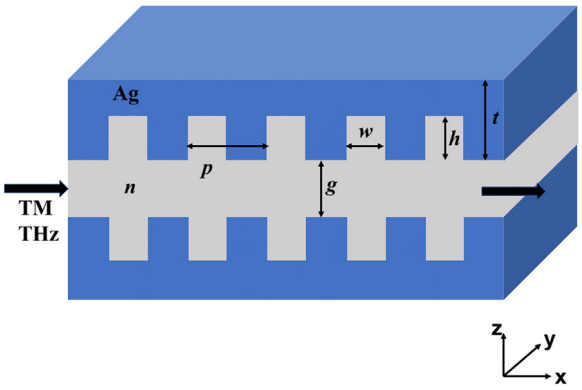

Fig. 1. Schematic illustration of the simulation structure. The y-dimension is assumed to be infinite. TM THz wave transmits parallel to the x-dimension.

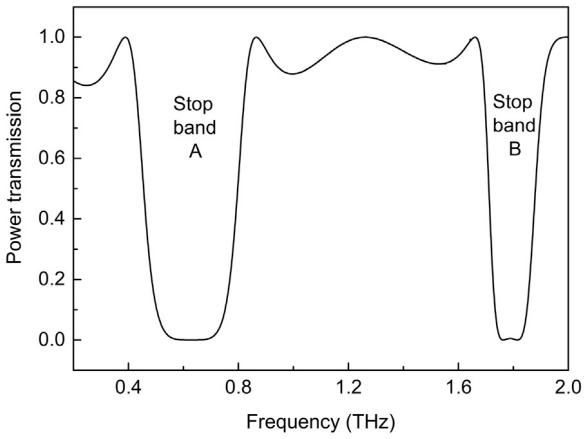

Fig. 2. A conventional power transmission spectrum of a PPWG. The main characteristic parameters are: g = 80 μm, h = 70 μm, p = 80 μm, m = 2, r = 0.5 and t = 1 mm.

is a perfect conductor [17] in THz frequency. The low-loss dielectric material fills as the waveguide, with a refractive index of n and the distance between inner surfaces of two plates is g. In order to obtain SPP mode, it is possible to embed various periodic structures, such as holes, columns, slits, and grooves [18–21]. The embedded periodic structures are highly sensitive to their geometry characteristics for SPP propagation [22]. Generally, the inner surfaces of two silver plates are etched with rectangular grooves with a period of p, which dictates the cutoff frequency of SPP. The depth and width of the grooves are h and w, respectively. The existence of stopband in the structure requires the grooves depth to be of the same order of magnitude as the period. The number of grooves is m, which affects the steepness of two stopbands. The duty cycle ratio (r) is ratio of the grating ridge dimension p-w to the period of grating p. The thickness of two uniform silver plates is t, where r = 0.5 and t = 1 mm are kept fixed. The typical geometry dimensions are markedly smaller than the operation wavelength, as deduced by considering mode generation. The transverse-magnetic (TM) linearly polarized pulsed THz wave is normally incident from the left input port of the device. Where the width of incident THz wave is equal to the width of input port, and the incident THz wave is assumed to be 100% coupled to the waveguide and transmitted parallel to the x-dimension. The proposed structure shows the one-dimensional periodic characteristic since the presence of corrugated groove arrays in x direction, the geometric model of the structure simulation can be simplified to a two-dimensional plane(x-z). Here, y-dimension is assumed to be infinite.

We are interested in the filter characteristic of 1 THz frequency; so, the related parameters are optimized for the propositional structure. With the help of finite element method, it is possible to calculate electromagnetic transmission properties through the filter in the THz domain [23]. Here, commercial software COMSOL Multiphysics is used. The values of different parameters such as g = 80 μm, h = 70 μm, p = 80 μm, m = 2, r = 0.5, and t = 1 mm. The conventional power transmission spectrum of the THz wave through the structure is shown in Fig. 2. As can be analyzed from Fig. 2, two stopbands exist in the transmission spectrum such as stopband A and stopband B. Stopband A locates in the low-frequency zone and is ascribed to the bandgap between SPP and waveguide mode. The SPP mode originates from the transformation of fundamental mode of waveguide mode in PPWG. Stopband B belongs to the bandgap of a high order waveguide which is located in high frequency zone. Sharp saltation occurs at the edge of two stopbands, during reflection and transmission. One transmission interval is sandwiched between two stopbands. The two stopbands can drift accordingly by adjusting the characteristic parameters of structure. If they meet face to face, then a narrow transmission peak forms at the border.

3. Stopband modulation analysis and simulation results

As mentioned earlier, the plate distance and grooves depth play an important role in the stopband drift. In order to understand the influence of plate distance (g), two stopbands were characterized as start-cutoff frequency (f_{sc}) and end-cutoff frequency (f_{ec}), respectively. Apart from plate distance, fixed parameters have been used where h = 35 μm, p = 80 μm, r = 0.5, t = 1 mm, m = 8, and n = 1.57. Unlike planar PPWG, both SPP mode and conventional waveguiding mode can be excited, depending on the plate distance in corrugated PPWG structure. The plate distance should be restricted in our proposed model, here its variation range of 20 μm to 120 μm to guarantee the two modes simultaneously existence in relevant frequency range of 0.2–2.0 THz. The position of two pairs of cutoff frequencies along with variation in plate distance is shown in Fig. 3, where h = 35 μm. Analysis of Fig. 3 concludes that bandwidth of stopband A becomes narrower as the distance of plate increases. On the other hand, cutoff frequency has different variation tendency: f_{scA} shifts to high frequency and becomes stable with the addition of g. So, it is found that plate distance finitely affects the interaction and coupling effect of SPP from the top and bottom surfaces of PPWG. In case of stopband B, the bandwidth variation is similar to stopband A. Both f_{scB} and f_{ecB} monotonously decrease along with the addition of g, while f_{scB} becomes stable at low frequency zone. In addition, the variation tendencies of f_{scB}, f_{ecB}, and f_{ecA} are opposite to that of f_{scA}. This behavior is due to the influence of plate distance on the waveguide modes. As the plate distance increases, the role of corrugated groove arrays diminishes, and the structure gradually trends to the planar PPWG without grooves arrays. The f_{scB} is close to f_{ecB}, it means the stopband B attributes of waveguide mode narrows, when the plate distance is larger but bounded, the stopband B even disappears (data not shown in Fig. 3). This trend agrees with conventional planar PPWG [15]. As discussed earlier, when the plate distance changes in the range of 20 μm to 120 μm, two stopbands gradually become close, junctures, and then moves away as plate distance increases. f_{scB} is almost tangential to f_{ecA} when the critical g value is near to 60 μm. So, an ultra-narrow passband will emerge under this condition.

The grooves depth can also affect the position of two stopbands. The position of two pairs of cutoff frequencies along with the variation in grooves depth, when g = 60 μm, is shown in Fig. 4. In case of f_{scB} and f_{ecB}, they show similar variation tendency as can be seen from Fig. 3. So, we can say that the influence of grooves depth is similar to the plate distance in stopband B. However, f_{scA} monotonously decreases along with the increase of h, which is opposite to that of Fig. 3. Furthermore, it indicates that the depth of the grooves has opposite effect on the SPP mode, compared to that of plate distance. In addition, f_{ecA} slowly

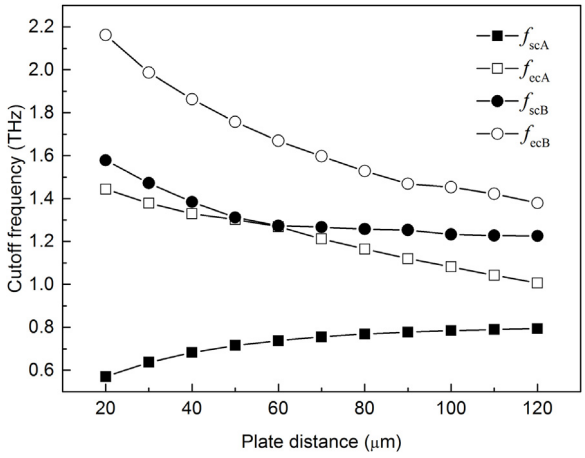

Fig. 3. Two pairs of cutoff frequencies as a function of plate distance when $h = 35$ μm ($p = 80$ μm, $r = 0.5$, $t = 1$ mm, $m = 8$, $n = 1.57$). The black squares mark represents the start-cutoff frequency of stopband A (f_{scA}); the void squares mark shows end-cutoff frequency of stopband A (f_{ecA}); the black circles mark shows the start-cutoff frequency of stopband B (f_{scB}); the void circles mark represents the end-cutoff frequency of stopband B (f_{ecB}).

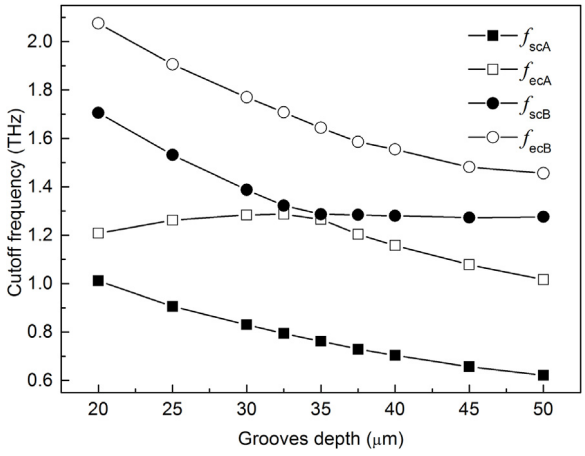

Fig. 4. Two pairs of cutoff frequencies as a function of the grooves depth when $g = 60$ μm ($p = 80$ μm, $r = 0.5$, $t = 1$ mm, $m = 8$, $n = 1.57$). The black squares: f_{scA}; void squares: f_{ecA}; black circles: f_{scB}; void circles: f_{ecB}.

climbs, followed by junctures with f_{scB} at the summit, and then drops down with the increase in grooves depth. It is concluded that stopband junction can be achieved from the adjustment of grooves depth.

The narrow band-pass filter based on a stopband modulation requires the two stopbands to be extremely close to each other, forming a slit-like shape. Their interval is extremely sensitive to the variation of grooves depth. The small deviation of grooves depth dramatically widens the interval. The behavior can result narrow band-pass filter which is invalid. In contrast, stopband interval slowly changes along with the variation of plate distance. In case of 10 GHz stopband interval, the approximate value is in the range of 50 to 65 μm in plate distance. It indicates that the plate distance has higher tolerances for the design of quality devices. Furthermore, by comparing Figs. 3 and 4, the variation trend of sideband suppression width (from f_{scA} to f_{ecB}) is different by the adjustments of plate distance and grooves depth. The width remains almost constant as the grooves depth changes. Nevertheless, the width will narrow as the plate distance increases. Given that sideband suppression width is sufficient, the plate distance more applicable to control the interval of two stopbands.

In order to verify the feasibility of narrow band-pass filter through stopband modulation, one narrow band-pass filter is demonstrated. The

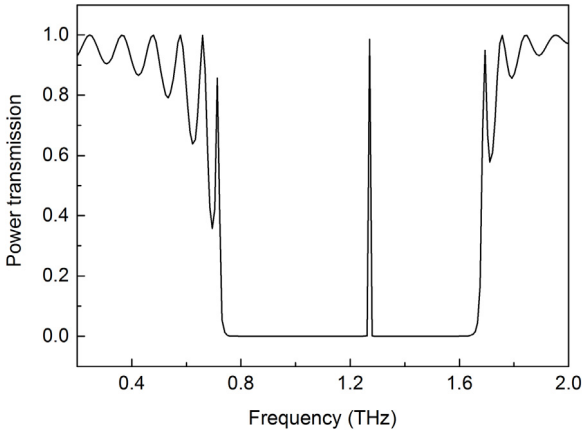

Fig. 5. Power transmission spectrum of THz wave through a filter with 62 μm plate distance and 35 μm grooves depth ($p = 80$ μm, $r = 0.5$, $t = 1$ mm, $m = 8$, $n = 1.57$).

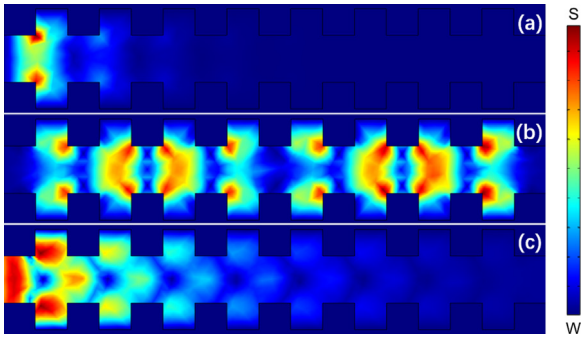

Fig. 6. Power field intensity distributions inside the filter. (a), (b), and (c) illustrate the power field intensity distributions at 1.0, 1.27, and 1.6 THz, respectively. S: strong, W: weak.

calculated transmission spectra of a PPWG with an optimized plate distance $g = 62$ μm is shown in Fig. 5. The THz wave is hindered with excellent cutoff feature within the broader THz frequency range from 0.75 to 1.65 THz. The corresponding energy cannot be transmitted through the device. However, only a single narrow band transmission peak with 1.27 THz exists in the wide stopband. This indicates that a single wave with 1.27 THz frequency can be transmitted and propagated through the device. Transmissivity is 99.8%, and the full width at half maximum (FWHM) of the passband is 5.8 GHz. Furthermore, the quality factor (the ratio of center frequency of peak to the FWHM) is Q ≈ 220, and a large range of sideband (900 GHz) equals to zero. Merely, because the adjustment scale of plate distance is micron order of magnitude, it needs to be handled carefully in practice, and if there is a displacement between the grooves, or there is small angle between the two plate, the spectrum quality of the pass band will be reduced.

Contour profiles of field distributions around PPWG area at different frequencies are shown in Fig. 6. Fig. 6(b) shows the power field intensity distribution inside the PPWG at a response frequency of 1.27 THz. Obviously, the incident TM wave evolves into an SPP wave on the edge of grooves in the PPWG; the SPP wave propagates along the waveguide with low energy loss and finally revivify into free-space THz wave, in the output port. The adjacent THz wave with other frequencies is hindered in PPWG. The reason behind this is, energy reflection or leakage i.e., the power field intensity distribution of 1.0 and 1.6 THz, as shown in Fig. 6(a) and (c). Furthermore, two different modes of THz waves are illustrated.

To analyze the tunable characteristic of frequency signal, we assumed that the waveguide cavity is filled with low loss nematic liquid crystal (LC) (E7, Merck) due to their relatively large birefringence

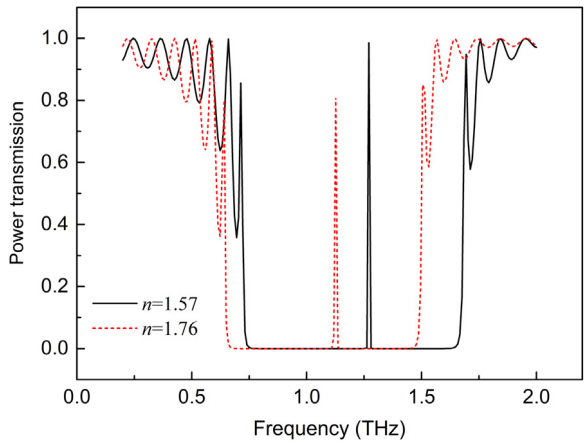

Fig. 7. Power transmission spectra for maximum and minimum of LC refractive index.

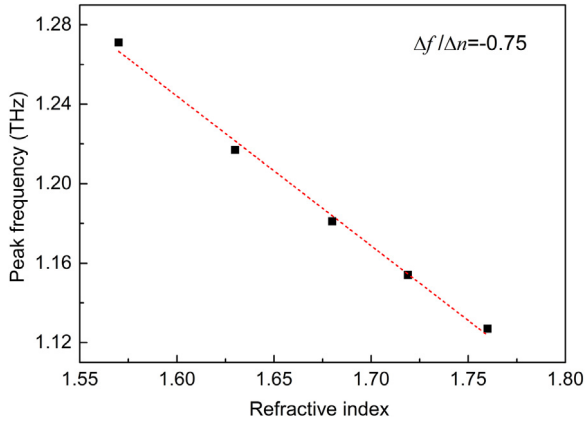

Fig. 8. Peak frequency shifts as a variation of effective index.

$\Delta n = n_e - n_o$. The ordinary and extraordinary refractive indices of E7 are 1.57 (n_o) and 1.76 (n_e), respectively, at around 1 THz [24]. If we assume a homogeneous alignment of the liquid crystal molecules, then the frequency shifts are in accord with the low voltage-controlled reorientation of the LC. By applying electric field, the frequency response of transmission spectrum shifts to low frequency such as from 1.27 to 1.13 THz with slightly transmission loss and constant linewidth (see Fig. 7).

The simulated transmission frequency of THz wave through a filter with different effective refractive index of LC is depicted in Fig. 8, where a near-linear relationship between response frequency shifts and the variation of refractive index is shown. The sensitivity of frequency tuning is given as $\Delta f/\Delta n = -0.75$ THz/RIU (RIU is the reflective index unit), where Δf is the peak frequency shifts and Δn is refractive index variation.

4. Conclusion

In summary, adjustments of plate distance and grooves depth, for the modulation of stopbands have been analyzed. It is found that this method of adjustment of plate distance is competent for the formation of narrow single passband. In addition, a high-quality band-pass filter is obtained at an optimized plate distance. The narrow frequency is selectively transmitted with a high Q-factor. However, the propagation loss in the proposed PPWG is not considered in the presented simulations and will be a subject of later studies. We also presented the designs of a tunable band-pass filter and modulate performance from the structure, utilizing the LC as an alterable waveguide dielectric. Numerical analysis showed that the proposed reconfigurable filter structure may be useful for the future all-integrated THz systems. Finally, we expect experimental verification by precisely controlling the plate distance.

CRediT authorship contribution statement

Kehui Jia: Conceptualization, Methodology, Formal analysis, Resources, Writing - original draft, Project administration. **Lina Fan:** Software, Investigation, Data curation, Writing - review & editing. **Zhaoliang Cao:** Investigation, Writing - review & editing.

Acknowledgment

The Project was supported by the State Key Laboratory of Applied Optics, Changchun Institute of Optics, Fine Mechanics and Physics, Chinese Academy of Sciences (No. 15020148).

References

[1] D.M. Mittleman, Twenty years of terahertz imaging, Opt. Express 26 (2018) 9417–9431, http://dx.doi.org/10.1364/OE.26.009417.
[2] N.J. Karl, R.W. McKinney, Y. Monnai, R. Mendis, D.M. Mittleman, Frequency-division multiplexing in the terahertz range using a leaky-wave antenna, Nat. Photonics 9 (2015) 717–720, http://dx.doi.org/10.1038/nphoton.2015.176.
[3] K.S. Reichel, P.Y. Lu, S. Backus, R. Mendis, D.M. Mittleman, Extraordinary optical transmission inside a waveguide: spatial mode dependence, Opt. Express 24 (2016) 28221–28227, http://dx.doi.org/10.1364/OE.24.028221.
[4] E.S. Lee, T.-I. Jeon, Tunable THz notch filter with a single groove inside parallel-plate waveguides, Opt. Express 20 (2012) 29605–29612, http://dx.doi.org/10.1364/OE.20.029605.
[5] K. Wang, Q. Cao, H. Zhang, P. Shen, L. Xing, Evanescent resonant mode for a T-shaped cavity in a terahertz parallel-plate waveguide, Appl. Opt. 57 (2018) 7967–7973, http://dx.doi.org/10.1364/AO.57.007967.
[6] L. Chen, Z.X. Cheng, J.M. Xu, X.F. Zang, B. Cai, Y.M. Zhu, Controllable multiband terahertz notch filter based on a parallel plate waveguide with a single deep groove, Opt. Lett. 39 (2014) 4541–4544, http://dx.doi.org/10.1364/OL.39.004541.
[7] A. Bingham, Y.G. Zhao, D. Grischkowsky, THz parallel plate photonic waveguides, Appl. Phys. Lett. 87 (2005) 051101, http://dx.doi.org/10.1063/1.1997273.
[8] S.P. Li, H.J. Liu, Q.B. Sun, N. Huang, A tunable terahertz photonic crystal narrow-band filter, IEEE Photonics Technol. Lett. 27 (2015) 752–754, http://dx.doi.org/10.1109/LPT.2015.2391127.
[9] H. Siampour, S. Kumar, V.A. Davydov, L.F. Kulikova, V.N. Agafonov, S.I. Bozhevolnyi, On-chip excitation of single germanium vacancies in nanodiamonds embedded in plasmonic waveguides, Light: Sci. Appl. 7 (2018) 61, http://dx.doi.org/10.1038/s41377-018-0062-5.
[10] H. Chen, H. Ma, Y. Li, J. Wang, Y. Han, M. Yan, S. Qu, Wideband frequency scanning spoof surface plasmon polariton planar antenna based on transmissive phase gradient metasurface, IEEE Antennas Wirel. Propag. Lett. 17 (2018) 463–467, http://dx.doi.org/10.1109/LAWP.2018.2795341.
[11] A. Vosoogh, A.U. Zaman, V. Vassilev, J. Yang, Zero-gap waveguide: A parallel plate waveguide with flexible mechanical assembly for mm-wave antenna applications, IEEE Trans. Compon. Packag. Manuf. Technol. 8 (2018) 2052–2059, http://dx.doi.org/10.1109/TCPMT.2018.2878643.
[12] P. Navaeipour, I. Al-Naib, M.M. Dignam, Third-harmonic terahertz generation from graphene in a parallel-plate waveguide, Phys. Rev. A 97 (2018) 013847, http://dx.doi.org/10.1103/PhysRevA.97.013847.
[13] S.R. Andrews, Microstructured terahertz waveguides, J. Phys. D: Appl. Phys. 47 (2014) 374004, http://dx.doi.org/10.1088/0022-3727/47/37/374004.
[14] C.I. Lin, T.K. Gaylord, Multimode metal–insulator–metal waveguides: Analysis and experimental characterization, Phys. Rev. B 85 (2012) 085405–1–085405–9, http://dx.doi.org/10.1103/PhysRevB.85.085405.
[15] J.A. Dionne, L.A. Sweatlock, H.A. Atwater, A. Polman, Plasmon slot waveguides: Towards chip-scale propagation with subwavelength-scale localization, Phys. Rev. B 73 (2006) 035407, http://dx.doi.org/10.1103/PhysRevB.73.035407.
[16] H.H. Tang, T.J. Ma, P.K. Liu, Experimental demonstration of ultra-wideband and high-efficiency terahertz spoof surface plasmon polaritons coupler, Appl. Phys. Lett. 108 (2016) 191903, http://dx.doi.org/10.1063/1.4948928.
[17] E.D. Palik, Handbook of Optical Constants of Solids, Academic Press, New York, 1998.
[18] W. Zhang, A. Charous, M. Nagai, D.M. Mittleman, R. Mendis, Extraordinary optical reflection resonances and bound states in the continuum from a periodic array of thin metal plates, Opt. Express 26 (2018) 13195–13204, http://dx.doi.org/10.1364/OE.26.013195.
[19] M. Wu, T. Lang, G. Shi, Z. Han, Generation and investigation of terahertz Airy beam realized using parallel-plate waveguides, Opt. Commun. 410 (2018) 520–524, http://dx.doi.org/10.1016/j.optcom.2017.10.039.

[20] E.S. Lee, J.-K. So, G.-S. Park, D. Kim, C.-S. Kee, T.-I. Jeon, Terahertz band gaps induced by metal grooves inside parallel-plate waveguides, Opt. Express 20 (2012) 6116–6123, http://dx.doi.org/10.1364/oe.20.006116.

[21] N. Bayat-Makou, A.A. Kishk, Realistic air-filled TEM printed parallel-plate waveguide based on ridge gap waveguide, IEEE Trans. Microw. Theory Techn. 66 (2018) 2128–2140, http://dx.doi.org/10.1109/TMTT.2018.2811487.

[22] M. Kuttge, F.J. García de Abajo, A. Polman, How grooves reflect and confine surface plasmon polaritons, Opt. Express 17 (2009) 10385–10392, http://dx.doi.org/10.1364/oe.17.010385.

[23] P. Neutens, P. Van Dorpe, I. De Vlaminck, L. Lagae, G. Borghs, Electrical detection of confined gap plasmons in metal–insulator–metal waveguides, Nat. Photonics 3 (2009) 283–286, http://dx.doi.org/10.1038/nphoton.2009.47.

[24] C.Y. Chen, C.F. Hsieh, Y.F. Lin, R.P. Pan, C.L. Pan, Magnetically tunable room-temperature 2π liquid crystal terahertz phase shifter, Opt. Express 12 (2004) 2625–2630, http://dx.doi.org/10.1364/opex.12.002625.